Improved distance analysis in RNA using network-editing techniques for overcoming errors due to spin diffusion

Charles G. Hoogstraten & Arthur Pardi*
Department of Chemistry and Biochemistry, Campus Box 215, University of Colorado, Boulder, CO 80309, USA

Abstract

Multispin magnetization transfer, or spin diffusion, is a significant source of error in NOESY-derived distance measurements for the determination of nucleic acid solution structures. The BD-NOESY and CBD-NOESY experiments, which allow the measurement of interproton distances with greatly reduced contributions from spin diffusion, have been adapted to structural analysis in RNA oligonucleotides. The techniques are applied to a lead-dependent ribozyme (LZ2). We demonstrate the measurement of both aromatic proton–aromatic proton NOEs free of spin diffusion involving the intervening ribose moieties and aromatic proton–ribose proton NOEs free of the efficient cross-relaxation within the ribose ring. In LZ2, the accuracy and precision of the resulting distances are significantly improved. We also find that, by allowing the use of longer mixing times with greater sensitivity, the experimental attenuation of spin diffusion in RNA increases the distance range of interactions that can be analyzed. This effect permits measurement of important long-range distances in LZ2 that are not accessible with standard techniques. Thus, these techniques allow the simultaneous optimization of the number, accuracy, and precision of distance constraints used for RNA structure determinations.

Introduction

The determination of high-resolution NMR solution structures of biological macromolecules relies on the measurement of interproton distances using NOESY experiments. A significant source of error in NOESY measurements is indirect magnetization transfer mediated by an intervening proton, termed spin diffusion, which generally leads to a systematic underestimation of longer distances (Kalk and Berendsen, 1976; Keepers and James, 1984; Hoogstraten and Markley, 1996a). Such problems are exacerbated in nucleic acids because the protons in the molecule are distributed unevenly in space (Wijmenga et al., 1993). Thus, many aromatic–aromatic and aromatic–ribose interproton distance measurements in DNA and RNA are badly perturbed by multispin effects.

The most common method for avoiding errors due to spin diffusion is the acquisition of a series of NOESY spectra at short mixing times, for which the initial slope yields a more trustworthy distance estimate (Anil Kumar et al., 1981). A major disadvantage of this initial rate method is the low sensitivity of NOESY experiments at short mixing times. In addition, acquisition of data at a number of mixing times may not be practical in the case of the three- and four-dimensional isotope-edited NOE spectra commonly used in larger macromolecules (Clore and Gronenborn, 1991).

In recent years, two broad classes of methods have been developed that attempt to overcome errors due to spin diffusion at longer mixing times, and thus make longer interproton distances amenable to NOE analysis. In the various types of matrix-based refinement (Boelens et al., 1988; Yip and Case, 1989; Borgias et al., 1990; Brüschweiler and Case, 1994), a preliminary analysis of NOESY data at long mixing times is combined with an initial structural model in an attempt to dissect the spin-diffusion pathways and produce a more accurate structural model. In contrast,

*To whom correspondence should be adressed.

the general approach of Magnetization Exchange Network Editing (MENE) involves the modification of the NOESY pulse sequence itself to eliminate certain spin-diffusion pathways (Macura et al., 1992, 1994; Hoogstraten and Markley, 1996a).

MENE experiments operate by considering the proton NMR spectrum as divided into two blocks, and either allowing cross relaxation within but not between blocks (Massefski and Redfield, 1988; Fejzo et al., 1991; Boulat et al., 1992; Burghardt et al., 1993; Hoogstraten et al., 1993; Zwahlen et al., 1994; Zolnai et al., 1995; Vincent et al., 1996a, b, 1997) or between but not within blocks (Fejzo et al., 1992; Hoogstraten et al., 1995b). These two classes of experiment are exemplified by BD-NOESY, which analyzes a large block of the spectrum free of spin diffusion mediated by protons in other spectral regions (Hoogstraten et al., 1993), and CBD-NOESY, which analyzes cross relaxation between two large spectral blocks while cancelling cross relaxation within each block (Hoogstraten et al., 1995b). A variety of studies have found improvements in derived macromolecular structures using various approaches to overcome spin diffusion (for a review, see Hoogstraten and Markley (1996a)).

Thus far, applications of MENE to nucleic acids have lagged behind those to proteins, despite the potentially serious problems due to spin diffusion in these systems. Recently, Bodenhausen and co-workers have reported the use of the QUIET-BAND-NOESY experiment in DNA to isolate the aromatic (H6/H8) and H2′/H2″ regions from all other protons (Vincent et al., 1996a). QUIET-BAND-NOESY, however, is less appropriate in RNA due to the limited dispersion of the ribose proton resonances. In this work, we demonstrate the application of the combination of various BD-NOESY and CBD-NOESY experiments for improved NOE analysis in RNA. The experimental system used is an *in vitro* selected lead-dependent autocleaving ribozyme (LZ2) that has been well characterized by NMR (Pan and Uhlenbeck, 1992a, b; Legault and Pardi, 1994; Pan et al., 1994; Legault, 1995; Mueller et al., 1995).

Materials and methods

For simulations of NOESY and BD-NOESY spectra, a model was derived from the crystallographic coordinates for the hammerhead ribozyme determined by McKay and co-workers (Pley et al., 1994). Protons were added to the X-ray coordinates with the program DISCOVER 95.0 (Molecular Simulations, Inc.) and the structure was energy-minimized to remove close contacts. Cross-relaxation simulations from nonexchangeable protons were performed using CORMA 5.0, modified to allow the zeroing of selected cross-relaxation rates for MENE simulations (Borgias et al., 1990; Liu et al., 1994; Hoogstraten and Markley, 1996b). Simulations used an isotropic correlation time of 6.0 ns, a spectrometer frequency of 600 MHz, CORMA default jump models, and a mixing time of 120 ms. BD-NOESY spectra were simulated by zeroing cross-relaxation rates connecting the H6/H8/H2 spin block with the ribose proton (including pyrimidine H5) spin block, and CBD-NOESY spectra were simulated by zeroing cross-relaxation rates within either of these spin blocks (Hoogstraten and Markley, 1996b). The deselected protons contributed to the autorelaxation in the same fashion as in NOESY. Observed NOEs within the aromatic block (NOESY and BD-NOESY) or between the aromatic block and ribose protons (NOESY and CBD-NOESY) were converted to interproton distances assuming that cross-relaxation rates were proportional to the inverse sixth power of the interproton distances. The median intensity in simulated NOESY spectra for pyrimidine H5-H6 proton pairs was set to a distance of 2.42 Å and used for calibration.

All NMR spectra were acquired on a 3.2 mM sample of LZ2 (Figure 2), prepared by *in vitro* transcription as previously described (Nikonowicz et al., 1992; Legault, 1995) and dissolved in a 10 mM pH 5.5 phosphate buffer in D_2O, 100 mM NaCl and 0.2 mM EDTA at a temperature of 25 °C. Prior to each use, the RNA sample was annealed by heating at 65 °C for 2 min and cooling on ice for 10 min. Spectra were acquired on a 500 MHz Varian UnityPlus spectrometer, except for the NOESY buildups, which were acquired on a 500 MHz Varian VXR spectrometer.

NOESY buildups were acquired with a proton carrier at 5.6 ppm, sweep widths of 4000 Hz in each dimension, 2048 complex points, low-power presaturation to attenuate residual HDO, and 220 complex t_1 points of 80 transients each. Spin-diffusion attenuated spectra were acquired using published pulse sequences for BD-NOESY (Hoogstraten et al., 1993), modified only by the addition of delays between selective inversions to reduce the number of pulses applied (Macura et al., 1994), and for CBD-NOESY (Hoogstraten et al., 1995b), used without modification. A key factor in the setup of these experiments is the choice

and careful adjustment of the band-selective inversion pulse used to divide the proton NMR spectrum into subdomains. Obtaining essentially perfect inversion within the desired bandwidth and minimal perturbation of the remainder of the proton resonances is critical to achieving satisfactory results (Hoogstraten and Markley, 1996a). For the case of CBD-NOESY, adjusting the precession delay to match the spin-lock power is also essential (Hoogstraten et al., 1995b). The BD-NOESY(arom-arom) buildup series was acquired with a proton carrier of 4.8 ppm, sweep widths in both dimensions of 6000 Hz, 2048 complex points, low-power presaturation of the residual HDO, and 256 complex t_1 points of 128 transients each. G^3 Gaussian cascade pulses of 3.2 ms (Emsley and Bodenhausen, 1990) were applied at 4.8 ppm every 40 ms during the mixing time. CBD-NOESY buildups were acquired with a proton carrier at 5.6 ppm, sweep widths of 4000 Hz in each dimension, 2048 complex points, low-power presaturation of the residual HDO, and 220 complex t_1 points of 80 transients each. During the mixing period, NOESY periods of $\tau_N = 30.6$ ms were alternated with ROESY periods of $\tau_R = 14.7$ ms; the reported 'mixing time' is $N(\tau_N + 2\tau_R)$, where N is the number of NOESY/ROESY cycles. ROESY spin-lock periods were flanked with 45.4 μs precession delays, to prevent signal losses due to repeated projection between the spin-lock axis and the xy plane, and 2.63 ms G^3 selective inversion pulses were applied at 4.8 ppm, to recouple the cross-relaxation interaction between spectral blocks (Hoogstraten et al., 1995b). A spin-lock power of 2750 Hz was used, and the entire cycle was repeated to give the desired mixing time. For both BD-NOESY and CBD-NOESY, a single z-gradient pulse at the beginning of the mixing time was used to remove undesired coherences.

BD-NOESY(arom-H1$'$), BD-NOESY(arom-ribo), and NOESY spectra were acquired at the single mixing time of 240 ms with the same pulse sequence and general setup as BD-NOESY(arom-arom). For BD-NOESY(arom-H1$'$), 6.7 ms G^3 pulses were applied at 4.1 ppm every 40 ms during the mixing time, whereas for BD-NOESY(arom-ribo), 5.8 ms G^3 pulses applied at 5.8 ppm were used. Presaturation at the HDO frequency was not used for these spectra. All NMR spectra were acquired using the States-TPPI method for quadrature detection in t_1 (Marion et al., 1989).

All NMR spectra were processed with FELIX 2.3.0 or 95.0 (Molecular Simulations, Inc.). Window functions of 3 Hz exponential line-broadening in t_2 and a cosine-squared bell in t_1 were used, with the

A: H6/H8, Ade H2
B: H1$'$ -- H5$'$/H5$''$, Pyr H5
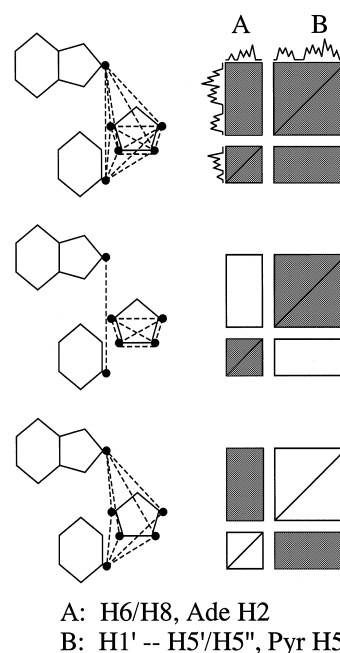
Figure 1. Schematic representations of cross relaxation for NOESY (top), BD-NOESY(arom-arom) (center) and CBD-NOESY (bottom). In these experiments, one spin block (A) contains the aromatic H2, H6, and H8 resonances and the other (B) contains all ribose protons and pyrimidine H5s. Protons considered are indicated as filled circles. Cross-relaxation processes active in a given pulse sequence are indicated as dashed lines superimposed on RNA oligomeric structure (sequential purine-pyrimidine base moieties and the intervening ribose ring) and as shaded regions in two-dimensional NMR spectra. H5$'$/H5$''$, AH2, and pyrimidine H5 protons are omitted for clarity.
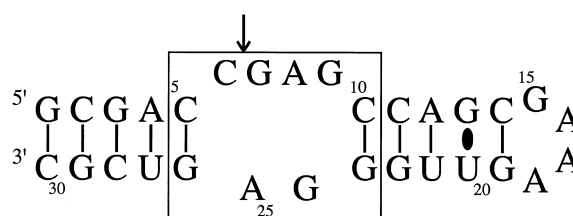
Figure 2. Secondary structure of LZ2, the lead-dependent ribozyme used for all spectroscopy in this paper. The autocleavage site is indicated with an arrow and the active-site internal loop is boxed.

t_1 data extended by 30–35% using linear prediction prior to application of the window. A final matrix size of 4096 × 1024 points was obtained in all cases, and residual baseline artifacts in ω_2 were removed by linear prediction of the first five complex points. Analysis of buildup curves for cross- to diagonal-peak ratios was performed by manual measurement of peak heights on extracted ω_2 (aromatic–aromatic NOEs only) or ω_1 vectors.
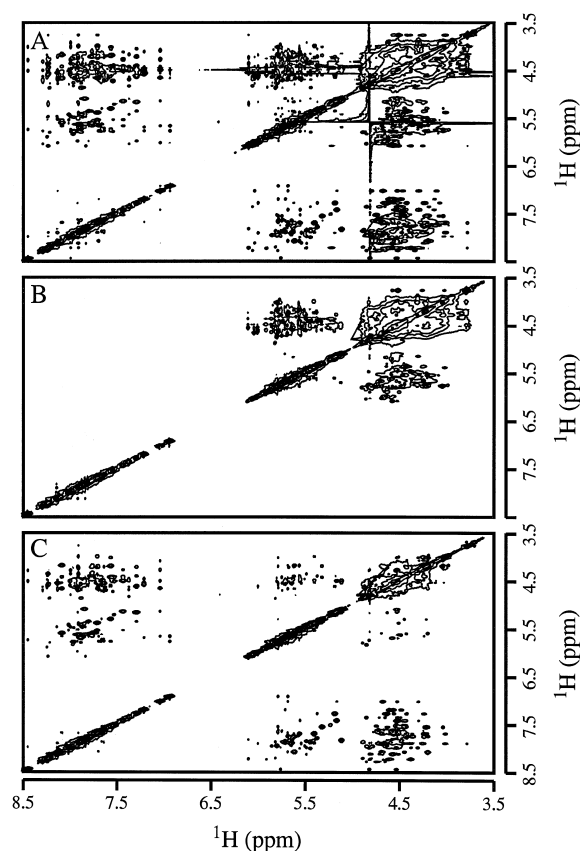
Figure 3. Two-dimensional cross-relaxation spectra of LZ2 in D_2O at 240 ms. Acquisition and processing were as described in the text. For plotting, contour levels were chosen such that the three spectra had equivalent apparent intensities for diagonal resonances in the aromatic region. (A) NOESY; (B) BD-NOESY(arom-arom); (C) CBD-NOESY.

Results and Discussion

Classification of MENE schemes used. The BD-NOESY experiment is implemented by using a band-selective pulse to repeatedly invert a spectral region during the NOESY mixing time; cross relaxation between spins within the pulse bandwidth and outside the bandwidth is cancelled. Spin-diffusion pathways involving protons within the pulse bandwidth do not contribute to cross peaks between protons outside the pulse bandwidth. In this work, we have implemented three forms of the BD-NOESY experiment in RNA by using various band-selective inversion pulses. For the BD-NOESY(arom-arom) implementation, a selective pulse tuned to invert the spectral region from 3.5 to 6.5 ppm (including the pyrimidine H5 and all ribose resonances but excluding the pyrimidine H6, purine H8, and adenine H2 aromatic resonances) is used. This

experiment allows the observation of NOEs between aromatic protons free of all spin diffusion mediated by ribose or H5 protons. BD-NOESY(arom-ribo) is implemented by inverting only the H1′ and pyrimidine H5 resonances (ca. 5.0 to 6.1 ppm) and analyzes NOEs between aromatic and non-H1′ ribose protons free of spin diffusion mediated by H1′ or H5 resonances. Finally, BD-NOESY(arom-H1′) is implemented by inverting only the non-H1′ ribose protons (ca. 3.7 to 5.0 ppm), and allows the analysis of NOEs among aromatic, H1′, and pyrimidine H5 resonances free of spin diffusion mediated by non-H1′ ribose protons. These considerations are summarized in Table 1.

CBD-NOESY is performed by alternating proton magnetization between the longitudinal and transverse frames in such a way as to cancel all cross relaxation, and using band-selective inversion pulses to reintroduce the NOE between the two spectral regions while maintaining the cancellation of cross relaxation within each region (Hoogstraten et al., 1995b). The CBD-NOESY experiment incorporating the same band-selective inversion pulse as BD-NOESY(arom-arom) allows the observation of aromatic–ribose NOEs free of the efficient magnetization transfer within the ribose ring. For example, intraresidue Harom-H1′ and Harom-H2′ NOEs may be independently measured free of the effects of rapid H1′-H2′ magnetization transfer. CBD-NOESY is thus the complement of the BD-NOESY(arom-arom) experiment, in that all cross peaks existing in a NOESY may be analyzed using one or the other of these sequences. The dissection of the cross-relaxation network in BD-NOESY(arom-arom) and CBD-NOESY is illustrated in Figure 1. Only spin-diffusion pathways contained completely within the H2/H6/H8 block will contribute intensity to the aromatic–aromatic peaks in BD-NOESY(arom-arom), and no two-step diffusive pathways can contribute to the aromatic–ribose peaks observed in CBD-NOESY (Figure 1, Table 1).

Simulations of network-editing spectra in RNA. Since the rigorous assessment of improvements in absolute accuracy is difficult in experimental situations, where the true structure is unknown, we have simulated NOESY, BD-NOESY(arom-arom), and CBD-NOESY spectra from a known RNA structure (Hoogstraten and Markley, 1996b). There is presently no X-ray or NMR structure for the lead-dependent ribozyme, so the X-ray structure of the hammerhead ribozyme (Pley et al., 1994) was used for simulations. Deviations between distances calculated from the simulated NOESY and MENE spectra

Table 1. Observed NOEs and active spin-diffusion pathways in cross-relaxation experiments in RNA

NOE type[a]	NOESY	BD-NOESY			CBD-NOESY
		(arom-arom)	(arom-H1′)	(arom-ribo)	
Aromatic–aromatic	yes	yes	yes	yes	no[b]
Aromatic-H1′/5	yes	no	yes	no	yes
Aromatic-H2′/3′/4′/5′	yes	no	no	yes	yes
Mediators of spin diffusion	all	none	H1′/H5	H2′/3′/4′/5′	none

[a] The presence or absence of cross peaks between aromatic (H2/H6/H8) protons and various proton classes is listed. Spin-diffusion pathways active for a given spectrum and cross-peak type are indicated; spin diffusion involving aromatic–aromatic transfer is neglected. Spin-diffusion pathways involving greater than two steps are not considered.

[b] Aromatic–aromatic cross peaks may arise in CBD-NOESY due to indirect transfer; these peaks are not directly useful in the derivation of distance constraints (see text).

and distances in the X-ray structure are analyzed in Table 2. The NOESY data are badly perturbed by a systematic underestimation of longer interproton distances. The maximum deviations are such that even a conservative bounds-setting protocol would lead to substantial numbers of constraints that were inaccurate in the sense of not containing the distance from the X-ray structure used for simulations, potentially leading to structural distortions. For the MENE data, both the rms and maximum errors in distance estimation are considerably decreased (Table 2), representing a significant improvement in distance accuracy. These data justify the use of tighter error bounds at a given mixing time than in the case of NOESY, for which upper bounds are typically loosened to allow for spin diffusion.

At a given mixing time, fewer cross peaks are observed in MENE data compared with NOESY (Table 2). This is largely due to the attenuation of spin-diffusion peaks in BD-NOESY or CBD-NOESY. Since spin diffusion typically requires the use of a shorter than optimal mixing time, however, the potential disadvantage of MENE experiments in reducing the number of distances analyzed may be overcome by the use of a longer mixing time (see below) (Hoogstraten and Markley, 1996b).

Network-editing spectra of LZ2. NOESY, BD-NOESY(arom-arom), and CBD-NOESY spectra of LZ2 are shown in Figure 3. BD-NOESY(arom-arom) spectra yield a rigorous cancellation of all cross-relaxation between the aromatic (H2/H6/H8) protons and the remainder of the proton spectrum. Since ribose-proton mediated spin-diffusion contributions to aromatic–aromatic NOEs are substantial at moderate mixing times, a striking overall decline in cross-peak
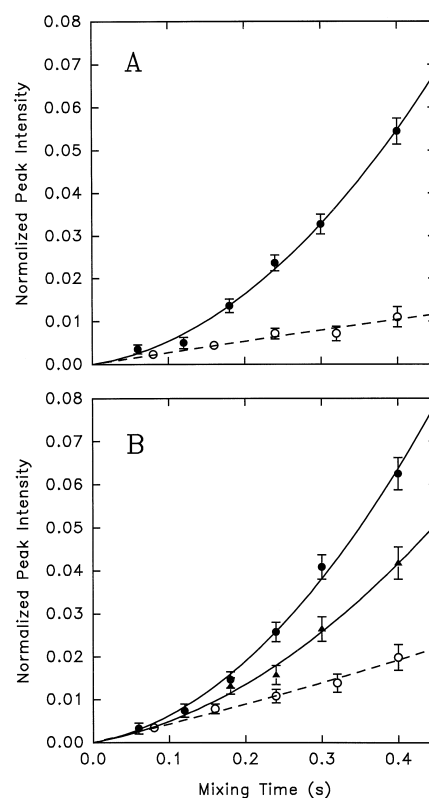
Figure 4. Normalized buildup curve analysis for NOESY (filled symbols, solid line) and BD-NOESY(arom-arom) (open symbols, dashed line) data on aromatic–aromatic NOEs in LZ2. Data points are cross- to diagonal-peak height ratios according to the prescription of Macura et al. (1986); lines represent fits to the equation $y = c_1 x + c_2 x^2$. Error bars are taken from the thermal noise level and thus only represent errors in peak quantitation. Absent bars represent error limits within the symbol size used for plotting. (A) G13 H8–A12 H8 (circle); (B) G26 H8–A25 H8 (circle), G26 H8–U27 H6 (triangle). The G26 H8–U27 H6 NOE was not observed at any mixing time in BD-NOESY.

Table 2. Analysis of accuracy of distances calculated from simulated cross-relaxation data sets

Spectrum	NOE type	Number observed[a]	Maximum deviation (Å)	Rms deviation (Å)
NOESY (120 ms)	aromatic–aromatic	62	2.34	0.628
BD-NOESY (120 ms)	aromatic–aromatic	53	0.458	0.172
NOESY (120 ms)	aromatic–ribose	459	2.38	0.634
CBD-NOESY (120 ms)	aromatic–ribose	387	0.836	0.122

[a] An NOE was considered to be observed if the corresponding cross peak had an intensity at least 0.1% of the hypothetical diagonal intensity for a single proton at zero mixing time.
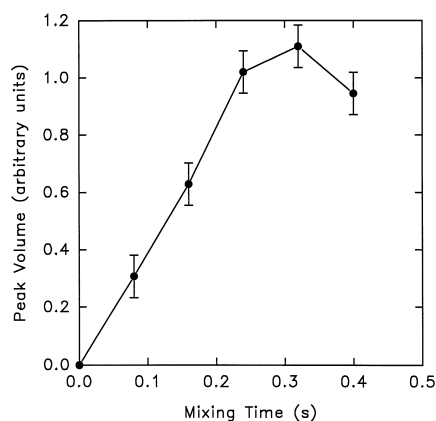
Figure 5. Integrated intensity for the A16 H8–A17 H8 NOE in BD-NOESY(arom-arom) spectra of LZ2 as a function of mixing time. Error bars are taken from the thermal noise level and thus only represent errors in peak quantitation.

intensity within the aromatic–aromatic region is also observed. In fact, most of the cross peaks analyzed in this work are beneath the contour level used in this figure. In the case of CBD-NOESY, cross peaks within each spectral block (aromatic or ribose) can arise due to multistep transfer (e.g., $H8_i - H2'_{i-1} - H6_{i-1}$), so that no regions of the spectrum are expected to be rigorously devoid of cross peaks.[1] Although we have not exploited this feature in the present work, the presence of a within-block cross peak in CBD-NOESY spectra may thus be diagnostic for the existence of a spin-diffusion pathway connecting the corresponding protons. As noted above, between-block cross peaks in CBD-NOESY spectra should be observed free of essentially all spin-diffusion contributions.

---

[1] Within-block cross peaks in CBD-NOESY may also arise due to Hartmann–Hahn transfer or off-resonance effects. We have ruled out these possibilities by varying the spin-lock power used during the ROESY delays, and therefore confirmed that these peaks arise from multistep transfer (data not shown).

Elimination of spin diffusion in aromatic–aromatic NOEs. In a plot of the cross- to diagonal-peak ratio for an NOE as a function of mixing time, direct cross relaxation will contribute linear normalized intensity, whereas spin diffusion gives rise to a quadratic or higher dependence (Macura et al., 1986). Since several aromatic resonances in LZ2 are completely resolved, we were able to verify directly the attenuation of spin-diffusion contributions in MENE as compared to NOESY by constructing normalized buildup curves.

Figure 4A shows such an analysis for a sequential aromatic proton–aromatic proton cross peak in an A-form duplex region of LZ2 (A12 H8–G13 H8). The NOESY buildup shows strong upward curvature, indicating a substantial spin-diffusion contribution presumably mediated by A12 H2′. An attempt to fit the linear portion of this curve would give a very poor determination of the linear term (the cross-relaxation rate). Use of a single NOESY spectrum at even a moderate mixing time would badly overestimate the cross-relaxation rate, and therefore badly underestimate the interproton distance. In contrast, the BD-NOESY buildup is linear to the longest mixing time used, indicating the presence of only direct NOE contributions. The slope of this line yields a distance estimate free of errors due to multispin effects. Similar effects are seen in Figure 4B, which shows NOEs involving a proton (G26 H8) within the active-site internal loop for LZ2. In this case, one NOE (G26 H8–U27 H6) that shows severe spin diffusion in the NOESY buildup is not detected at all in BD-NOESY, indicating that this interproton distance is longer than the detection limit for this system, and even a generous distance constraint would lead to errors and possible structural distortion. For the sequential G26 H8–A25 H8 NOE within the active-site internal loop of LZ2, both NOESY and BD-NOESY buildups closely resemble those seen for the comparable A12–G13 step, supporting a standard helical
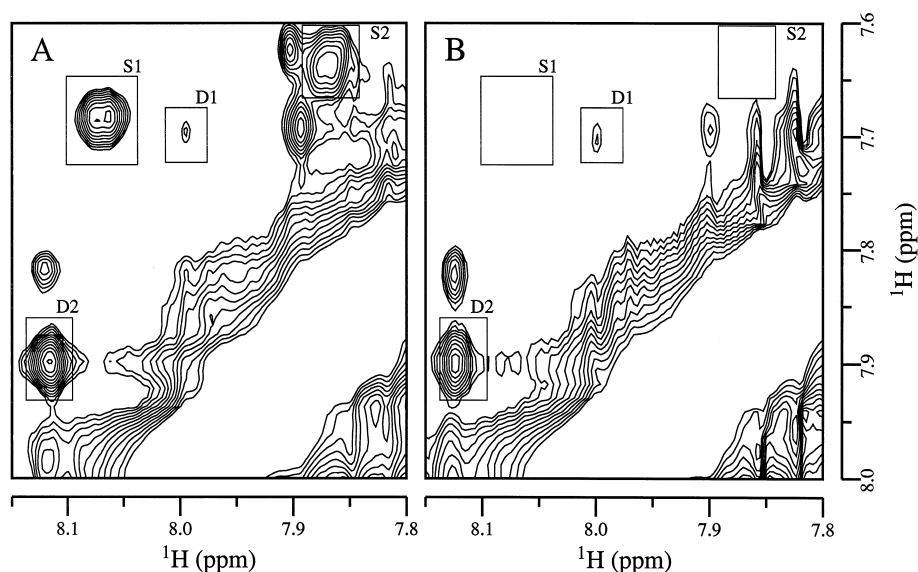
Figure 6. Sections of the aromatic region of two-dimensional 240 ms (A) NOESY and (B) BD-NOESY(arom-arom) spectra of LZ2 in D_2O. Contour levels were set such that the two spectra had equivalent apparent intensity for aromatic proton diagonal resonances. Positive levels only are shown. Peaks D1 and D2 are primarily due to direct cross relaxation as shown by their similar intensity in both spectra; peaks S1 and S2 are primarily due to spin-diffusion contributions as shown by their strong diminution in BD-NOESY. Peak assignments: D1, A25 H2–G7 H8; D2, A12 H8–C11 H6; S1, U21 H6–G22 H8; S2, C28 H6–G29 H8.

conformation for these residues. BD-NOESY analysis of aromatic–aromatic NOEs in RNA essentially eliminates spin diffusion, allowing the mixing time used to be chosen based on considerations of sensitivity alone.

The advantages of the use of longer mixing times in the absence of spin diffusion are shown in Figure 5, which displays the absolute (i.e., not normalized by the diagonal intensity) buildup curve for a weak NOE (A16 H8–A17 H8) observed in the BD-NOESY(arom-arom) buildup series of LZ2. The optimum sensitivity for this cross peak is obtained at approximately 300 ms, well above the region at which NOESY data are usable. The location of the cross-peak sensitivity maximum varies from cross peak to cross peak, generally occurring at longer mixing times for longer interproton distances (Macura, 1994). Thus, BD-NOESY allows the optimization of the experiment for the detection of critical long-distance interactions.

An example of the use of long-mixing time NOE data is shown in Figure 6, which compares 240 ms NOESY and BD-NOESY(arom-arom) spectra of LZ2. Some cross peaks in the NOESY are eliminated or drastically attenuated in the BD-NOESY whereas others are observed at essentially full intensity in BD-NOESY as compared to NOESY. The former peaks arise largely from spin diffusion and the latter peaks largely from direct cross relaxation. In particular,

the spin-diffusion peaks S1 and S2 are among the strongest resonances in this spectral region in NOESY, but are essentially eliminated by the BD-NOESY procedure. This demonstrates that the major contribution to these NOEs is spin diffusion through ribose proton(s). Peak D2, in contrast, is observed at the same strong intensity in both spectra, demonstrating that this correlation is dominated by direct NOE contributions. Interestingly, peak D1, a key cross-strand NOE within the internal loop of LZ2, is confirmed as a direct NOE by BD-NOESY at this relatively long mixing time. At the shorter mixing times required to eliminate spin-diffusion contributions to NOESY, this peak is not observable. Thus, BD-NOESY has improved the sensitivity of NOE analysis by allowing the use of longer mixing times. At these longer mixing times, an important interproton distance that was completely inaccessible by standard techniques has become amenable to analysis.

Elimination of spin diffusion in aromatic–ribose NOEs using CBD-NOESY. The elimination of spin-diffusion contributions to aromatic–ribose NOEs is illustrated by comparison of the intensity of cross peaks to G23 H8 in the ω_2 vectors from the 240 ms NOESY and CBD-NOESY spectra, shown in Figure 7. The intraresidue aromatic–H1′ connectivity (labeled I) has
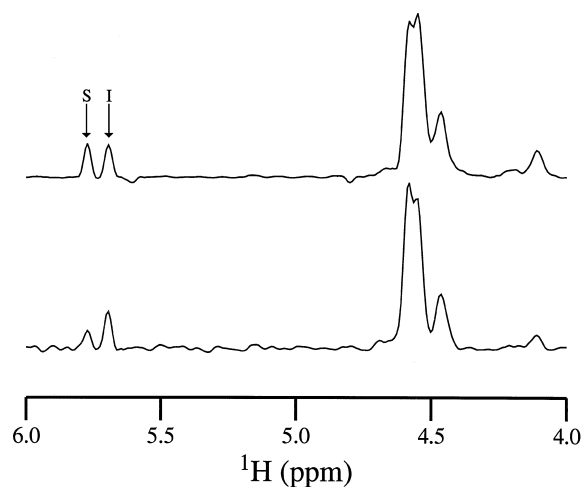
Figure 7. Vectors through 240 ms NOESY (top) and CBD-NOESY (bottom) spectra of LZ2 in D$_2$O at the ω_2 frequency of G23 H8. The intraresidue (G23 H1′) and sequential (G22 H1′) aromatic-H1′ NOEs are labeled I and S, respectively.

essentially the same intensity in the CBD-NOESY as compared to the NOESY spectrum. By contrast, the sequential aromatic-H1′ cross peak (labeled S) is substantially decreased in intensity in CBD-NOESY, indicating a major spin-diffusion contribution to this cross peak in NOESY. In A-form helical regions, an efficient spin-diffusion pathway exists for this contact due to the short sequential aromatic-H2′ distance (Wij-menga et al., 1993). CBD-NOESY has eliminated this indirect contribution by suppressing cross relaxation between the H1′ and H2′ atoms of G22. CBD-NOESY, therefore, allows analysis of all aromatic–ribose NOEs unperturbed by the efficient cross relaxation within the ribose moiety.

The elimination of spin diffusion in CBD-NOESY is further illustrated in Figure 8, which plots the normalized buildup curves for sequential and intraresidue aromatic-H1′ cross peaks to guanine residues 23 and 26 in CBD-NOESY compared to NOESY. The NOESY data show significant spin-diffusion contributions, as diagnosed by upward curvature of the buildup, whereas the CBD-NOESY data are linear to the longest mixing time tested. Although in A-form helices the intraresidue and sequential aromatic-H1′ distances are significantly different (ca. 3.6 Å vs. 4.3 Å), these cross peaks have indistinguishable intensities in the 120 ms NOESY spectrum. CBD-NOESY, by contrast, allows the longer sequential distance to be clearly distinguished from the shorter intraresidue distance, and either the slopes of the buildup curves
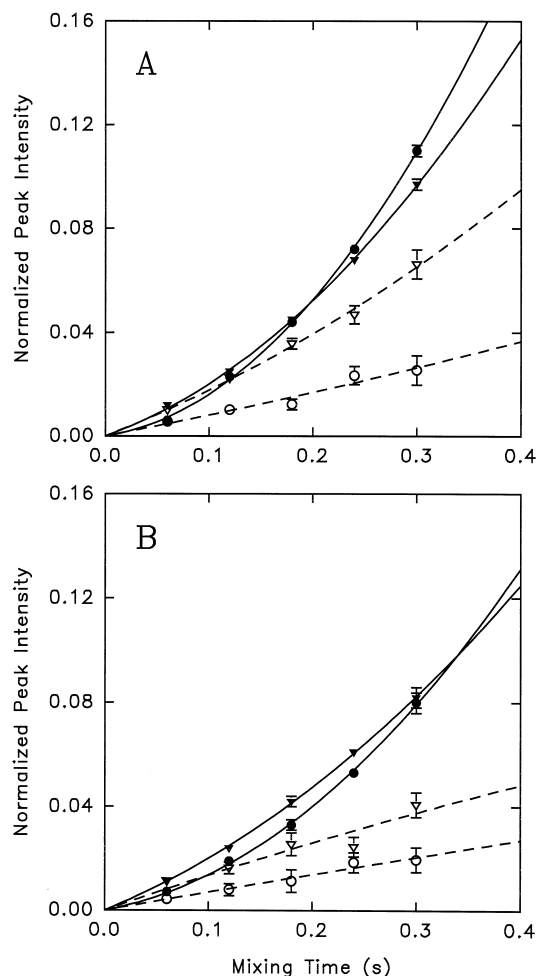
Figure 8. Normalized buildup curve analysis for NOESY (filled symbols, solid line) and CBD-NOESY (open symbols, dashed line) data on aromatic-H1′ NOEs in LZ2. Data analysis and presentation are as described for Figure 4. (A) Intraresidue (G23 H1′, triangle) and sequential (G22 H1′, circle) NOEs to G23 H8. (B) Intraresidue (G26 H1′, triangle) and sequential (A25 H1′, circle) NOEs to G26 H8.

or appropriately calibrated analysis of a single mixing time can give a more accurate measurement of each distance. The ability to distinguish a 3.6 Å from a 4.3 Å distance illustrates the improved precision of CBD-NOESY measurements.

Analysis of aromatic–ribose NOEs using BD-NOESY. In a BD-NOESY experiment the spins of interest are not manipulated directly; therefore, the sensitivity is comparable to that of NOESY experiments. For CBD-NOESY, however, one-half of the cross relaxation takes place in the rotating frame, which dramatically accelerates the autorelaxation in macromolecules. A
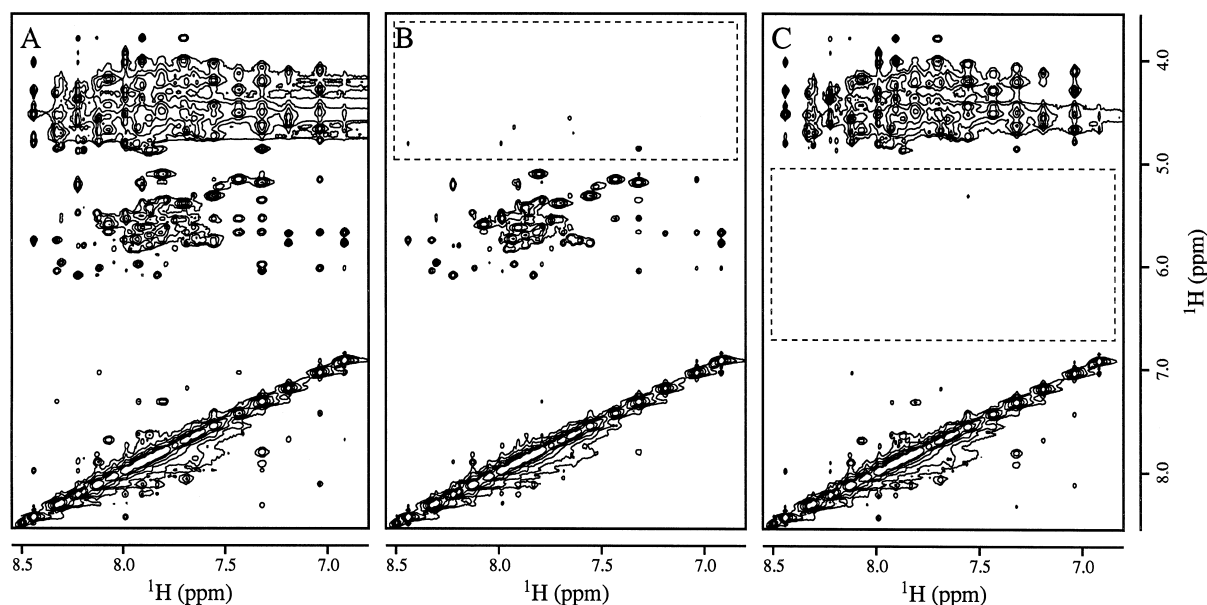
Figure 9. Sections of two-dimensional 240 ms (A) NOESY, (B) BD-NOESY(arom-H1′), and (C) BD-NOESY(arom-ribo) spectra of LZ2 in D$_2$O. Spectra were acquired under identical instrumental conditions and plotted at the same contour level to compare the sensitivities of the three experiments. Dashed boxes indicate spectral regions corresponding to suppressed cross-relaxation interactions.

CBD-NOESY experiment designed to be comparable to a 200 ms NOESY, for example, will involve approximately 50 ms of spin-lock, leading to a substantial loss in sensitivity for larger macromolecules. In the case of CBD-NOESY, therefore, improvements in the accuracy and precision of distance measurement are possible, but the sensitivity advantages of operating at longer mixing times are not realized. Methods to measure aromatic-ribose NOEs with decreased spin diffusion but using the greater sensitivity of BD-NOESY are therefore desirable. The BD-NOESY(arom-H1′) experiment is particularly advantageous for analyzing aromatic-H1′ NOEs, given the efficient spin diffusion often mediated by H2′ protons. By contrast, the BD-NOESY(arom-ribo) experiment allows confirmation of *syn* base conformations by measurement of intraresidue aromatic-H2′ NOEs independent of spin diffusion mediated by the H1′ resonance.

Sections of two-dimensional NOESY, BD-NOESY (arom-H1′), and BD-NOESY(arom-ribo) spectra of LZ2 at 240 ms are presented in Figure 9. The cancellation of cross peaks corresponding to deselected pathways (regions enclosed by dashed boxes) is clearly seen. The signal-to-noise in both BD-NOESY experiments is degraded by less than 10% compared to NOESY, although some peaks near the transition region of the selective inversion pulse are affected to

a greater extent. A more detailed picture is seen in the comparison of vectors through G13 H8 in Figure 10. Essentially total elimination of deselected cross peaks is seen. Relatively small changes are observed between NOESY and BD-NOESY(arom-ribo) in the remaining regions for this vector. The BD-NOESY(arom-H1′) spectrum, however, displays a noticeable decline in signal in the sequential aromatic-H1′ NOE (labeled S), which, as discussed above, is expected to be perturbed by efficient spin diffusion through the H2′ resonance for this A-RNA region of LZ2. Thus, this experiment has allowed a very useful reduction in major spin-diffusion pathways without the sensitivity disadvantages of CBD-NOESY. Interestingly, the sequential aromatic–aromatic NOEs visible in the NOESY spectrum are also strongly attenuated in the BD-NOESY(arom-H1′) spectrum but retained in the BD-NOESY(arom-ribo) data; these observations are consistent with a substantial contribution to these peaks due to spin diffusion via non-H1′ ribose protons (particularly H2′ atoms), and emphasize the key role played by the proton-dense ribose moiety in spin-diffusion pathways in RNA. We expect the BD-NOESY(arom-H1′) scheme to be useful for the analysis of aromatic–aromatic and aromatic-H1′ NOEs in three-dimensional heteronuclear-edited experiments, allowing a combination of improved ac-
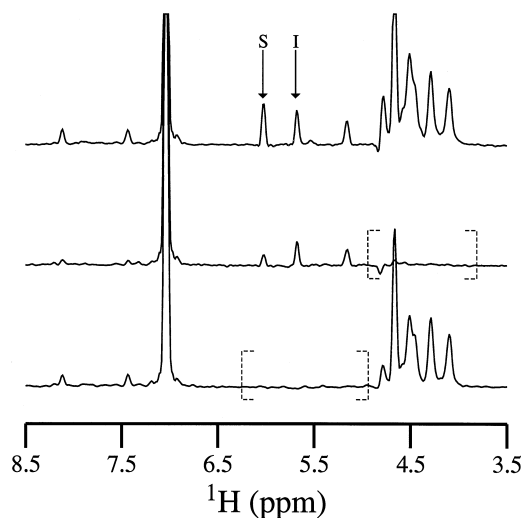
Figure 10. Sections through the spectra shown in Figure 9 at the ω_2 frequency of G13 H8: NOESY (top), BD-NOESY(arom-H1′) (center), and BD-NOESY(arom-ribo) (bottom). Intraresidue (G13 H1′) and sequential (A12 H1′) NOEs are labeled I and S, respectively. Vectors are plotted at the same absolute scale. Dashed brackets indicate spectral regions corresponding to suppressed cross-relaxation interactions. Intensity loss for peak I in BD-NOESY (arom-H1′) compared to NOESY is due to the spin-diffusion contribution to this NOE at 240 ms (see Figure 8).

curacy, excellent peak dispersion, and sensitivity improvements due to the use of mixing times near the optimum for weak NOEs.

Conclusions

Multistep magnetization transfer, or spin diffusion, can lead to serious systematic inaccuracies in interproton distances determined via NMR. To account for these inaccuracies, NOESY data are taken at shorter mixing times, reducing the sensitivity of the experiment, and low-precision distance bounds are used in the structure calculations. In this paper, we have demonstrated experimental schemes that reduce or eliminate spin diffusion for aromatic–aromatic and aromatic–ribose proton NOEs in RNA oligomers. The BD-NOESY and CBD-NOESY experiments allow the measurement of interproton distances in RNA with much greater accuracy than standard techniques. In addition, in NOESY, a weak cross peak may indicate either a spin-diffusion pathway or a weak but direct interaction, whereas BD-NOESY and CBD-NOESY allow these two situations to be distinguished. In this paper, we have demonstrated these points largely by

analysis of NOESY and MENE data in regions of known structure and spin-diffusion pathways; the results obtained justify confidence in MENE data for other regions, such as the asymmetric internal loop in LZ2, for which the structure is not currently known. By justifying the use of tighter error limits, network-editing data can also improve the precision of applied distance constraints. Finally, the high sensitivity of the BD-NOESY experiment at longer mixing times increases the upper distance limit of interactions that can be analyzed, resulting in useful data for proton pairs that cannot be analyzed by NOESY. Thus, appropriately designed network-editing experiments can simultaneously improve the accuracy, precision, and number of structural constraints.

In RNA, relatively long aromatic proton–aromatic proton or aromatic proton–H1′ distances are often perturbed by spin diffusion through the intervening proton-dense ribose ring. BD-NOESY(arom-arom) or BD-NOESY(arom-H1′) effectively suppress the effects of non-H1′ ribose protons on such NOEs, resulting in a much simpler relaxation network in which spin diffusion is greatly attenuated. By contrast, CBD-NOESY allows the distance from a given aromatic proton to each proton within a ribose ring to be accurately determined by removing all cross relaxation within a ribose ring, increasing the number of independent distance measurements possible. Since BD-NOESY will be more sensitive than CBD-NOESY for larger oligonucleotides, but the elimination of spin diffusion is more complete in CBD-NOESY, the choice of approach for studying aromatic–ribose NOEs will depend on the experimental system.

Finally, we emphasize that BD-NOESY and CBD-NOESY pulse sequences differ from the standard NOESY method only in the pulses applied during the mixing time. Therefore, these mixing sequences are fully compatible with multidimensional, heteronuclear-edited NOESY spectra, allowing a combination of improved peak dispersion and attenuation of spin diffusion (Hoogstraten et al., 1995a). By allowing reliable distance constraints to be derived from data taken at a single sensitivity-optimized mixing time, three-dimensional MENE experiments are a more practical approach than the acquisition of buildup curves of three- or four-dimensional data. Due to the severity of the spin-diffusion problem in large nucleic acids, these experimental approaches for the removal of spin diffusion represent an important addition to the methodology of nucleic acid solution structure determination.

Acknowledgements

References

Anil Kumar, Wagner, G., Ernst, R.R. and Wüthrich, K. (1981) *J. Am. Chem. Soc.*, **103**, 3654–3658.

Boelens, R., Koning, T.M.G. and Kaptein, R. (1988) *J. Mol. Struct.*, **173**, 299–311.

Borgias, B.A., Gochin, M., Kerwood, D.J. and James, T.L. (1990) *Prog. NMR Spectrosc.*, **22**, 83–100.

Boulat, B., Burghardt, I. and Bodenhausen, G. (1992) *J. Am. Chem. Soc.*, **114**, 10679.

Brüschweiler, R. and Case, D.A. (1994) *Prog. NMR Spectrosc.*, **26**, 27–58.

Burghardt, I., Konrat, R., Boulat, B., Vincent, S.J.F. and Bodenhausen, G. (1993) *J. Chem. Phys.*, **98**, 1721–1736.

Clore, G.M. and Gronenborn, A.M. (1991) *Science*, **252**, 1390–1399.

Emsley, L. and Bodenhausen, G. (1990) *Chem. Phys. Lett.*, **165**, 469–476.

Fejzo, J., Westler, W.M., Macura, S. and Markley, J.L. (1991) *J. Magn. Reson.*, **92**, 195–202.

Fejzo, J., Westler, W.M., Markley, J.L. and Macura, S. (1992) *J. Am. Chem. Soc.*, **114**, 1523–1524.

Hoogstraten, C.G., Westler, W.M., Macura, S. and Markley, J.L. (1993) *J. Magn. Reson.*, **B102**, 232–235.

Hoogstraten, C.G., Choe, S., Westler, W.M. and Markley, J.L. (1995a) *Protein Sci.*, **4**, 2289–2299.

Hoogstraten, C.G., Westler, W.M., Macura, S. and Markley, J.L. (1995b) *J. Am. Chem. Soc.*, **117**, 5610–5611.

Hoogstraten, C.G. and Markley, J.L. (1996a) In Jardetzky, O. and Lefevre, J.F. (Eds), *NATO/ASI Series: Dynamics and the Problem of Recognition in Biological Macromolecules*, Plenum, New York, NY, pp. 73–111.

Hoogstraten, C.G. and Markley, J.L. (1996b) *J. Mol. Biol.*, **258**, 334–348.

Kalk, A. and Berendsen, H.J.C. (1976) *J. Magn. Reson.*, **24**, 343–366.

Keepers, J.W. and James, T.L. (1984) *J. Magn. Reson.*, **57**, 404–426.

Legault, P. (1995) *Structural Studies of Ribozymes by Heteronuclear NMR Spectroscopy (Ph.D. Thesis)*, University of Colorado, Boulder, CO.

Legault, P. and Pardi, A. (1994) *J. Am. Chem. Soc.*, **116**, 8390–8391.

Liu, H., Anil Kumar, Borgias, B.A., Thomas, P.D. and James, T.L. (1994) *CORMA 5. 0/MARDIGRAS 3. 0 (UCSF)*, University of California, San Francisco, CA.

Macura, S., Farmer II, B.T. and Brown, L.R. (1986) *J. Magn. Reson.*, **70**, 493–499.

Macura, S., Fejzo, J., Hoogstraten, C.G., Westler, W.M. and Markley, J.L. (1992) *Isr. J. Chem.*, **32**, 245–256.

Macura, S. (1994) *J. Magn. Reson.*, **B104**, 168–171.

Macura, S., Westler, W.M. and Markley, J.L. (1994) *Methods Enzymol.*, **239**, 106–144.

Marion, D., Ikura, M., Tschudin, R. and Bax, A. (1989) *J. Magn. Reson.*, **85**, 393–399.

Massefski Jr., W. and Redfield, A.G. (1988) *J. Magn. Reson.*, **78**, 150–155.

Mueller, L., Legault, P. and Pardi, A. (1995) *J. Am. Chem. Soc.*, **117**, 11043–11048.

Nikonowicz, E.P., Sirr, A., Legault, P., Jucker, F.M., Baer, L.M. and Pardi, A. (1992) *Nucleic Acids Res.*, **20**, 4507–4513.

Pan, T., Dichtl, B. and Uhlenbeck, O.C. (1994) *Biochemistry*, **33**, 9561–9565.

Pan, T. and Uhlenbeck, O.C. (1992a) *Biochemistry*, **31**, 3887–3895.

Pan, T. and Uhlenbeck, O.C. (1992b) *Nature*, **358**, 560–563.

Pley, H.W., Flaherty, K.M. and McKay, D.B. (1994) *Nature*, **372**, 68–74.

Vincent, S.J.F., Zwahlen, C. and Bodenhausen, G. (1996a) *J. Biomol. NMR*, **7**, 169–172.

Vincent, S.J.F., Zwahlen, C., Bolton, P.H., Logan, T.M. and Bodenhausen, G. (1996b) *J. Am. Chem. Soc.*, **118**, 3531–3532.

Vincent, S.J.F., Zwahlen, C., Post, C.B., Burgner, J.W. and Bodenhausen, G. (1997) *Proc. Natl. Acad. Sci. USA*, **94**, 4383–4388.

Wijmenga, S.S., Mooren, M.M.W. and Hilbers, C.W. (1993) In Roberts, G.C.K. (Ed.), *NMR of Macromolecules: A Practical Approach*, Oxford Univ. Press, Oxford, pp. 217–288.

Yip, P. and Case, D.A. (1989) *J. Magn. Reson.*, **83**, 643–648.

Zolnai, Z., Juranic, N., Markley, J.L. and Macura, S. (1995) *Chem. Phys.*, **200**, 161–179.

Zwahlen, C., Vincent, S.J.F., Di Bari, L., Levitt, M.H. and Bodenhausen, G. (1994) *J. Am. Chem. Soc.*, **116**, 362–368.